J. Fluid Mech. (1999), *vol.* 378, *pp.* 145–166. Printed in the United Kingdom

Three-dimensional instability of Burgers and Lamb–Oseen vortices in a strain field

By CHRISTOPHE ELOY AND STÉPHANE LE DIZÈS

Institut de Recherche sur les Phénomènes Hors Équilibre, UMR 6594, CNRS, Universités d'Aix-Marseille I et II, 12, avenue Général Leclerc, F-13003 Marseille, France

(Received 28 July 1997 and in revised form 20 July 1998)

The linear stability of Burgers and Lamb–Oseen vortices is addressed when the vortex of circulation Γ and radius δ is subjected to an additional strain field of rate s perpendicular to the vorticity axis. The resulting non-axisymmetric vortex is analysed in the limit of large Reynolds number $R_\Gamma = \Gamma/\nu$ and small strain $s \ll \Gamma/\delta^2$ by considering the approximations obtained by Moffatt *et al.* (1994) and Jiménez *et al.* (1996) for each case respectively. For both vortices, the TWMS instability (Tsai & Widnall 1976; Moore & Saffman 1975) is shown to be active, i.e. stationary helical Kelvin waves of azimuthal wavenumbers $m = 1$ and $m = -1$ resonate and are amplified by the external strain in the neighbourhood of critical axial wavenumbers which are computed. The additional effects of diffusion for the Lamb–Oseen vortex and stretching for the Burgers vortex are proved to limit in time the resonance. The transient growth of the helical waves is analysed in detail for the distinguished scaling $s \sim \Gamma/(\delta^2 R_\Gamma^{1/2})$. An amplitude equation describing the resonance is obtained and the maximum gain of the wave amplitudes is calculated. The effect of the vorticity profile on the instability characteristic as well as of a time-varying stretching rate are analysed. In particular the stretching rate maximizing the instability is calculated. The results are also discussed in the light of recent observations in experiments and numerical simulations. It is argued that the Kelvin waves resonance mechanism could explain various dynamical behaviours of vortex filaments in turbulence.

1. Introduction

Interest in vortex dynamics has been renewed by the discovery of strong vorticity filaments in turbulent flows (Cadot, Douady & Couder 1995; Vincent & Meneguzzi 1991). These localized structures could play an important role in the statistical properties of turbulence (Lundgren 1982) and explain its intermittent character (Jiménez *et al.* 1993). It is thus legitimate to try to understand the fundamental mechanisms governing the dynamics of such structures, and more precisely to determine their stability, which is the subject of this paper.

For the last thirty years, vortex stability analyses have focused on axisymmetrical vortices with axial flow (see for instance the review of Ash & Khorrami 1995) in order to explain the so-called 'vortex breakdown' phenomenon observed experimentally in pipes (Sarpkaya 1971), cylinders with rotating ends (Escudier 1984) and on delta wings (Peckham & Atkinson 1957). Saffman (1992) has conjectured that the same phenomenon could explain the bursting of vortex filaments in turbulence but a complete theory is still lacking. Moreover, it is still unclear whether vortices in turbulent flows exhibit a mean axial flow which is required for 'vortex breakdown'. In this paper, we shall consider vortices without mean axial flow.

Vortex filaments have been generally associated with axisymmetric vortices for which the vorticity is simultaneously concentrated by axial stretching and diffused by viscosity. The simplest models are the famous Burgers vortex which is the equilibrium vortex configuration in a uniform stretching field, and the Lamb–Oseen vortex which is an unstretched diffusing vortex. Recent works have shown the influence on intense vortex filaments of a pure shear flow (Kawahara *et al.* 1998) or a non-uniform axisymmetric strain field (Verzicco, Jiménez & Orlandi 1995). Non-axisymmetric solutions were obtained by Moffatt, Kida & Ohkitani (1994) and Jiménez, Moffatt & Vasco (1996) (see also Ting & Tung 1965) by submitting the Burgers and Lamb–Oseen vortices to an additional plane strain field with principal axes perpendicular to the vortex axis. Non-axisymmetric corrections were calculated in the limit of large Reynolds numbers. They were shown to induce interesting modifications in the energy dissipation distribution which are in remarkably good agreement with what has been observed in numerical simulations of two- and three-dimensional turbulence (see Jiménez *et al.* 1996 and Moffatt *et al.* 1994 respectively). However, filaments are also known to exhibit a rich variety of dynamical behaviour which includes bursting, spliting and merging (see Arendt, Fritts & Andreassen 1998, for instance). It is then natural to address the question of the stability of the above solutions.

So far, the very few existing stability analyses have in general considered the Burgers and Lamb–Oseen vortices without external strain. Bernoff & Lingevitch (1994) analysed the two-dimensional stability of the Lamb–Oseen vortex: they showed that the vortex relaxes on a time scale faster than the viscous time scale to an axisymmetric state when perturbed. More results have been obtained for the Burgers vortex but a complete three-dimensional stability analysis is still lacking. Robinson & Saffman (1984) and Prochazka & Pullin (1995) showed the stability with respect to two-dimensional perturbations. These results were recently extended by Prochazka & Pullin (1998) for a non-axisymmetric vortex. Using energy methods, Leibovich & Holmes (1981) proved that no finite critical viscosity guarantees the global decreasing of the perturbations of the Burgers vortex. Rossi & Le Dizès (1997) analysed the effect of the stretching field on the axial wavenumber of the perturbations. They showed that the discrete part of the temporal spectrum of any stretched vortex can only be associated with perturbations without axial dependency.

One of the main effects of imposing an additional external strain, perpendicular to the vortex axis, is to modify the form of the vortex core from circular to elliptical (Robinson & Saffman 1984; Moffatt *et al.* 1994; Jiménez *et al.* 1996). Such an effect is expected to be destabilizing since the elliptical character of the streamlines is indeed known to be a source of instability (Pierrehumbert 1986). This so-called 'elliptical instability' has been put on firm ground in the context of a pure elliptical flow by Bayly (1986), Landman & Saffman (1987), Waleffe (1990) and Lifschitz & Hameiri (1991) who interpreted the instability mechanism as a parametric excitation of inertial waves. Their analysis has also been extended to more complex configurations to account for stratification (Miyazaki & Fukumoto 1992), Coriolis effects (Craik 1989; Cambon *et al.* 1994), stretching (Le Dizès, Rossi & Moffatt 1996) time-dependency (Foster & Craik 1996; Bayly, Holm & Lifschitz 1996) and non-uniform vorticity profile (Leblanc & Cambon 1998; Sipp & Jacquin 1998). Very few experiments have been designed to study the elliptical instability and only qualitative results have been published so far (Vladimirov & Tarasov 1982; Malkus 1989; Gledzer & Ponomarev 1992). However, this instability is now recognized as a fundamental instability which could explain the three-dimensional transition of numerous flows such as wakes (Williamson 1996; Leweke & Williamson 1998*b*), mixing layers (Landman & Saffman 1987) and vortex pairs (Leweke & Williamson 1998*a*).

Surprisingly, the elliptical instability has not immediately been related to the short-wave instability identified by Widnall, Bliss & Tsai (1974) in vortex rings and analysed by Tsai & Widnall (1976) or Moore & Saffman (1975) in the context of two-dimensional inviscid vortices in a weak external strain field (see the presentation of both instabilities in Saffman 1992). Tsai & Widnall (1976) considered the case of a Rankine vortex. They showed that stationary helical waves of azimuthal wavenumbers $m = -1$ and $m = 1$ are amplified for certain values of their wavenumber by the external strain field. Moore & Saffman (1975) interpreted this instability as a resonance phenomenon and gave a formal extension of Tsai & Widnall's analysis to a large class of non-viscous two-dimensional vortices. Although Waleffe (1990) did not point out the connection, his analysis permits the Tsai–Widnall–Moore–Saffman (TWMS) instability and the elliptical instability to be linked. He formed, from a superposition of most unstable inertial waves, the resonant helical modes of Tsai & Widnall (1976) in the Rankine vortex core. He also calculated the maximum growth rate of the inertial waves and obtained a value comparable to the growth rate given in Tsai & Widnall (1976) for the resonant helical waves. This explains why the combination of helical waves $m = -1$ and $m = +1$ is the most unstable mode for the elliptically perturbed Rankine vortex. For more realistic vortices, the connection between both instabilities is not as simple. It would require the use of more sophisticated techniques (Bayly *et al.* 1996) to extend the elliptical instability to a non-uniform vorticity profile. Contrarily to the Rankine vortex, it is then not guaranteed that the stationary helical waves analysed in Moore & Saffman (1975) for a large class of vortices constitute the most unstable mode. Despite this point which is discussed again in the last section, Moore & Saffman's (1975) analysis is useful to obtain sufficient conditions of instability. In this paper we shall demonstrate that their analysis applies to a large family of stretched vortices which includes the Burgers and Lamb–Oseen vortices if the external strain field acting on the vortices is small and if the Reynolds number is large.

This paper is organized as follows. The analysis and the results are first presented for Burgers and Lamb–Oseen vortices (§2–§4) and then extended to a large class of arbitrary stretched vortices in §5–§6. In §2, the basic flow solution is presented. In particular, the corrections to the Burgers and Lamb–Oseen vortices due to the external strain are given. Section 3 starts with a simple description of the instability mechanism following Moore & Saffman's (1975) analysis. The additional effects of viscosity and stretching are then discussed: they are shown to limit in time the growth of the resonant helical waves. This leads to a rough estimate for the maximum gain of the wave amplitude. In §4, an asymptotic analysis of the instability is carried out for the distinguished scaling that gives an $O(1)$ gain. An amplitude equation describing the resonance is obtained as well as a precise value for the gain. The instability characteristics are analysed in §5. The influence of the vorticity profile on the local growth rate is first discussed. Then, the effect of the stretching field on the maximum gain is considered. For this purpose, a generalization of the analysis to an arbitrarily stretched vortex is carried out. In the last section, the general results are presented in the context of turbulent flows.

2. Burgers and Lamb–Oseen vortices in a non-axisymmetric strain field

Burgers and Lamb–Oseen vortices are both axisymmetric Gaussian vortice solutions of the incompressible Navier–Stokes equations. They are respectively stretched and unstretched along their axis (the z-axis hereafter). They both admit an axial vorticity

field of the form

$$\omega_z = \frac{\Gamma}{\delta^2} G\left(\frac{r}{\delta}\right), \tag{2.1}$$

where G is the normalized Gaussian function:

$$G(x) = \frac{1}{4\pi} \mathrm{e}^{-x^2/4}. \tag{2.2}$$

They are characterized by their circulation Γ and radius δ. For the Burgers vortex, the radius is $\delta_B = (\nu/\gamma)^{1/2}$ where ν is the kinematic viscosity and γ the stretching rate of the external stretching field $\boldsymbol{U}_\gamma = (-\frac{1}{2}\gamma x, -\frac{1}{2}\gamma y, \gamma z)$. The Burgers vortex corresponds to the equilibrium configuration for which the spreading of vorticity due to viscous diffusion is exactly balanced by the concentration process induced by stretching. The Lamb–Oseen vortex is only subject to viscous diffusion; its radius δ_L increases with time according to $\delta_L = (\nu t)^{1/2}$ while its circulation Γ remains constant.

When an external strain field $\boldsymbol{U}_s = (sx, -sy, 0)$ is added perpendicularly to the vortex axis, the axisymmetric vortex is no longer a solution of the Navier–Stokes equations. However, in the limit of large Reynolds numbers ($R_\Gamma = \Gamma/\nu$), an asymptotic study shows that the main features of the vortex are conserved near its core. In the case of the Lamb–Oseen vortex, Ting & Tung (1965) were the first to calculate the vorticity corrections due to the strain. Their asymptotic analysis has been recently re-examined and compared to two-dimensional numerical simulations of vortical structures in turbulent flows by Jiménez *et al.* (1996). For the Burgers vortex, the analysis has been carried out by Moffatt *et al.* (1994). Like Ting & Tung (1965) and Jiménez *et al.* (1996), they obtained in the high Reynolds numbers limit a first order correction to the vorticity distribution (2.1) proportional to the strain rate s. For both vortices, the axial vorticity has a similar expression which reads

$$\omega_z = \frac{\Gamma}{\delta^2} G\left(\frac{r}{\delta}\right) + s\eta\left(\frac{r}{\delta}\right) F\left(\frac{r}{\delta}\right) \sin 2\theta + O\left(\frac{s\gamma\delta^2}{\Gamma}, \frac{s^2\delta^2}{\Gamma}\right), \tag{2.3}$$

where

$$\eta(x) = \frac{x^2}{4\left(\mathrm{e}^{x^2/4} - 1\right)}, \tag{2.4}$$

and $F(x)$ satisfies

$$\frac{\mathrm{d}^2 F}{\mathrm{d}x^2} + \frac{1}{x}\frac{\mathrm{d}F}{\mathrm{d}x} - \frac{4}{x^2} F + \eta(x) F = 0. \tag{2.5}$$

The function F is subject to the boundary conditions $F(x) \sim s_0 x^2/4$ near zero and $F(x) \sim x^2/4$ near infinity, which yields, after numerical integration, $s_0 \approx 2.525$. The function F measures the interaction of the vortex with the strain field. In particular, the ratio $4F(x)/x^2$ which is displayed on figure 1 gives near 0 and $+\infty$ the non-axisymmetric part of the strain rate. It shows that the strain rate near 0 is more than 2.5 times the strain rate at infinity. We shall see in §5 the importance of this result in interpreting the instability characteristics.

The full velocity and pressure field associated with (2.3) is

$$V_r = s\delta^2 \frac{4F(r/\delta)}{r} \cos 2\theta - \frac{\gamma}{2} r + O\left(s^2\delta^3/\Gamma, s\gamma\delta^3/\Gamma\right), \tag{2.6a}$$

$$V_\theta = \frac{\Gamma}{\delta} V(r/\delta) - 2s\delta F'(r/\delta) \sin 2\theta + O\left(s^2\delta^3/\Gamma, s\gamma\delta^3/\Gamma\right), \tag{2.6b}$$

$$V_z = \gamma z, \tag{2.6c}$$

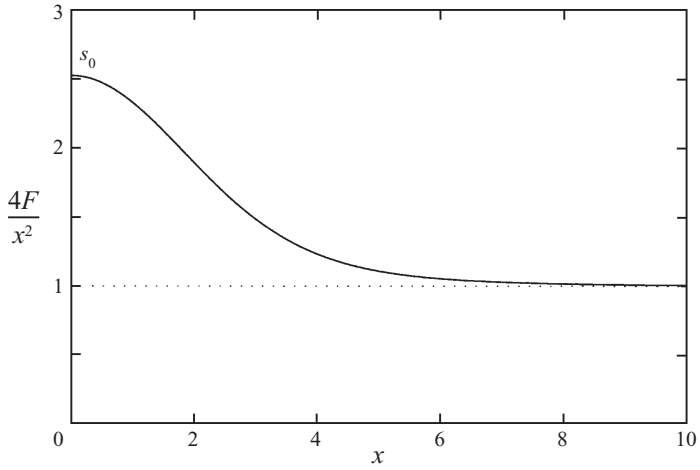

FIGURE 1. Plot of $4F/x^2$ as a function of x. Near 0 and $+\infty$, this function gives the non-axisymmetric part of the strain rate because F is proportional to x^2.

$$P = -\frac{\Gamma^2}{2\delta^2}\left[V(r/\delta)\right]^2 + s\frac{\Gamma}{\delta}F'(r/\delta)V(r/\delta)\sin 2\theta + O(s^2\delta, s\gamma\delta), \tag{2.6d}$$

where $V(x)$ is the azimuthal velocity profile of the Burgers and Lamb–Oseen vortices:

$$V(x) = \frac{1 - \mathrm{e}^{-x^2/4}}{2\pi x}. \tag{2.7}$$

The validity of approximation (2.6*a–d*) is discussed in Moffatt *et al.* (1994), Jiménez *et al.* (1996) and Prochazka & Pullin (1998). As long as $\Gamma/\delta^2 \gg s$ and $\Gamma/\delta^2 \gg \gamma$ (this second condition is always satisfied for the Lamb–Oseen vortex since $\gamma = 0$), the approximation is valid in the vortex core and can be applied up to $r = O([\Gamma/(\delta^2 s)]^{1/4}\delta)$. As explained in Jiménez *et al.* (1996), the domain of validity can be extended, by an adequate modification of the coordinates, up to $r = O([\Gamma/(\delta^2 s)]^{1/2}\delta)$, which corresponds to the limit of the region dominated by vorticity. For larger r, the strain field becomes dominant and the vorticity is no longer axisymmetric at leading order. Prochazka & Pullin (1998) recently obtained an approximation of the flow in that region. For the Burgers case, Moffatt *et al.* (1994) discussed the nature of the approximation according to the value of the parameter $\lambda \equiv 2s/\gamma$ which measures the departure from axisymmetry in the strain field. For $0 < \lambda < 1$ (non-axisymmetric axial strain) the vorticity presumably remains stationary and tends to the expression obtained by Robinson & Saffman (1984): $\omega_z \propto \exp[(s - \gamma/2)x^2 - (s + \gamma/2)y^2]$. By contrast, for $\lambda > 1$ (bi-axial strain), the vorticity field is expected to become time-dependent for large r, and to be 'stripped away' in the direction of positive strain (x-direction with the above notation). Moffatt *et al.* (1994) evaluated the time scale of this process and concluded that the vortex (defined by the expressions (2.6*a–d*)) could survive an exponential long time before being ultimately destroyed. This analysis was refined and corrected by Prochazka & Pullin (1998) but they reached the same conclusion. In the present study, we shall not consider the description of the vortex in the far field, since this region, where the vorticity is already exponentially small, has a negligible influence on the instability process described below.

For future use, in §5, it is important to point out that (2.3) and (2.6*a–d*) are also

valid if γ varies slowly or if γ is different from 0 (Lamb–Oseen vortex) or δ^2/ν (Burgers vortex). However, in such cases, the vortex radius has a particular time evolution which will be calculated in §5.

3. Instability mechanism

Let us assume for the moment that stretching and viscous diffusion are negligible. Expression (2.3) for the vorticity field derived in the previous section then describes a two-dimensional, inviscid and stationary vortex. The stability of such vortices with respect to particular three-dimensional perturbations was analysed in a general setting by Moore & Saffman (1975). The main ideas of their analysis can be applied to the present case as follows.

In the limit of small external strain ($s \ll \Gamma/\delta^2$), the vorticity is given, at leading order, by expression (2.1). The property of axisymmetry of this expression guarantees that Kelvin waves can be added, as neutral perturbations, to the basic flow. Such waves are of the form:

$$\boldsymbol{v} = \Phi(r)\mathrm{e}^{\mathrm{i}(kz-\omega t+m\theta)} + \text{c.c.}, \tag{3.1}$$

where the frequency ω is related to the axial and azimuthal wavenumbers k and m through the dispersion relation $D(\omega, k, m) = 0$.

The effect of the strain field on these perturbations can be apprehended by rewriting the strain field in cylindrical coordinates: $\boldsymbol{U}_s = (sr\cos 2\theta, -sr\sin 2\theta, 0)$. Indeed, this expression shows that the interaction of a Kelvin wave of azimuthal wavenumber m with the strain field generates two additional waves of azimuthal wavenumbers $m \pm 2$ (see also the next section). As a consequence, the two waves m and $m+2$ resonate via the strain when they satisfy $D(\omega, k, m) = D(\omega, k, m+2) = 0$. Using the symmetry property of the dispersion relation, i.e. $D(\omega, k, m) = D(-\omega, k, -m)$, Moore & Saffman (1975) deduced that stationary helical waves ($\omega = 0$ and $m = \pm 1$) satisfy the above resonance condition for any dimensionless axial wavenumber κ such that $D(0, \kappa/\delta, 1) = 0$. They proved that this particular combination of helical modes is always amplified by the strain and gives rise to an instability. This result was simultaneously obtained by Tsai & Widnall (1976) for the Rankine vortex. Referring to both studies, we shall henceforth name it the 'Tsai–Widnall–Moore–Saffman (TWMS) instability'. This instability is characterized by a growth rate $\sigma = O(s)$ and a band $\Delta\kappa = O(s\delta^2/\Gamma)$ of unstable dimensionless wavenumbers $k\delta$ around the critical values κ.

The main effect of viscosity and stretching is to introduce a transient aspect to this instability. Let us first discuss the case of the unstretched Lamb–Oseen vortex. For such a vortex, the radius δ_L increases as $(\nu t)^{1/2}$, i.e. on a time scale $t_L = O(\delta^2/\nu) = O(\delta^2 R_\Gamma/\Gamma)$. So, if we start from an unstable configuration of helical waves, after a finite period of time, $k\delta$ leaves the unstable band around a critical wavenumber κ and the helical waves are no longer unstable (see sketch in figure 2*a*). In other words, the growth of the unstable helical waves is only transient. The gain of amplitude G of these waves across the unstable domain can be roughly estimated as $G \propto \exp(\tau\sigma)$, where τ is the time spent in the unstable band and σ the mean growth rate of the instability. Here $\tau = O((\Delta\kappa)t_L) = O\left(sR_\Gamma\delta^4/\Gamma^2\right)$ and $\sigma = O(s)$. The gain of amplitude is then of the form $G \propto \exp\left(s^2R_\Gamma\delta^4/\Gamma^2\right)$. If $s \gg \Gamma/\left(\delta^2R_\Gamma^{1/2}\right)$, the gain of amplitude of the helical waves is expected to be exponentially large: the vortex can be considered as unstable.

For the Burgers vortex, stretching plays the same role as diffusion by modifying the

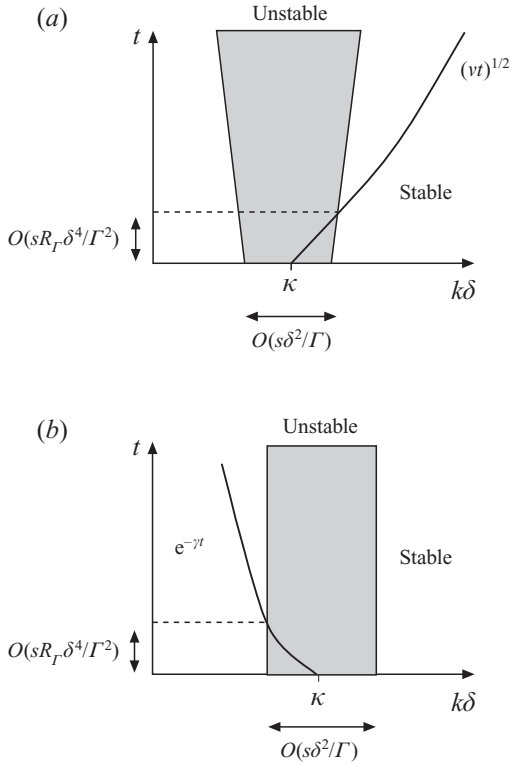

FIGURE 2. Time evolution of the product $k\delta$ for the Lamb–Oseen vortex (*a*) and for the Burgers vortex (*b*). In both cases, $k\delta$ remains a finite time in the unstable band around κ.

wavenumber of the perturbations. Indeed, if we consider an arbitrary perturbation, the action of the stretching field $\boldsymbol{U}_\gamma = (-\frac{1}{2}\gamma x/-\frac{1}{2}\gamma y)$ is to decrease its axial wavenumber according to $k_B = k_0 \exp(-\gamma t)$. Such an evolution is the consequence of a degeneracy for large z which requires the conservation of the phase factor e^{ikz} for any wave in the stretching field $\boldsymbol{U}_\gamma$:

$$\left(\frac{\partial}{\partial t} + \boldsymbol{U}_\gamma \cdot \nabla\right) e^{ikz} = 0. \tag{3.2}$$

This result has already been used by Craik & Criminale (1986) and Lifschitz & Hameiri (1991) for the local stability analysis of flows near stagnation points. It is also the main ingredient of Rossi & Le Dizès (1997).

As for the Lamb–Oseen vortex, if we start from an unstable configuration of helical waves, after a finite time of order $\tau = \Delta\kappa/\gamma = O(sR_\Gamma\delta^4/\Gamma^2)$, the product $k\delta$ would leave the unstable band $\Delta\kappa$ (see sketch in figure 2*b*). The growth is then also transient and the same conclusion holds for the Burgers vortex: it is unstable if $s \gg \Gamma/(\delta^2 R_\Gamma^{1/2})$. Since the Burgers vortex radius is $\delta = (\nu/\gamma)^{1/2}$, this case corresponds to a strong bi-axial strain configuration with $s/\gamma \gg R_\Gamma^{1/2}$. In particular, if $s \sim \gamma$, the stretching ensures the stability of the Burgers vortex with respect to the TWMS instability. Note however that, when $2s > \gamma$, the vortex is also subject to a tilting instability (Prochazka & Pullin 1998) which tends to align the vortex axis with the direction of maximum extensional strain. The time scale $O((s-\gamma)^{-1})$ of this instability is comparable to the TWMS instability time scale when $s \gg \gamma$. But the tilting instability is a nonlinear

phenomenon for an infinite vortex as it requires a finite-amplitude perturbation to modify by an infinitesimal angle the direction of the vortex axis. It will not be considered in the following analysis.

In the next section, a more detailed analysis of the TWMS instability is carried out. More specifically, the maximum gain of amplitude of the helical waves is computed for both the Burgers and the Lamb–Oseen vortices for the distinguished scaling $s \sim \Gamma/(\delta^2 R_\Gamma^{1/2})$.

4. Asymptotic analysis for the distinguished scaling

Let us consider a Burgers or Lamb–Oseen vortex in a strain field of rate s (at infinity) such that

$$s^* \equiv \frac{2s\delta^2 R_\Gamma^{1/2}}{\Gamma} = O(1). \tag{4.1}$$

Using dimensionless quantities (the characteristic time and space variables are δ^2/Γ and δ respectively), expressions (2.6*a–d*) for the velocity and pressure field reduce to

$$V_r = \varepsilon s^* \frac{2F(r^*)}{r^*} \cos 2\theta + O(\varepsilon^2), \tag{4.2a}$$

$$V_\theta = \frac{1 - \mathrm{e}^{-r^{*2}/4}}{2\pi r^*} - \varepsilon s^* F'(r^*) \sin 2\theta + O(\varepsilon^2), \tag{4.2b}$$

$$V_z = O(\varepsilon^2) \quad (\varepsilon^2 z \text{ for Burgers and 0 for Lamb–Oseen}), \tag{4.2c}$$

$$P = -\frac{1}{2}\left(\frac{1 - \mathrm{e}^{-r^{*2}/4}}{2\pi r^*}\right)^2 + \varepsilon s^* F'(r^*) V_0(r^*) \sin 2\theta + O(\varepsilon^2), \tag{4.2d}$$

where the small expansion parameter is defined by $\varepsilon = R_\Gamma^{-1/2}$. In (4.2*a–d*), r^* (stars are dropped thereafter) denotes the dimensionless radial coordinate. For the Lamb–Oseen vortex, this coordinate is time-varying due to the evolution of the dimensionless δ as $\delta_L = \varepsilon t^{1/2}$ (note that for $t = t_0 = R_\Gamma$, $\delta_L = 1$).

The axial component V_z is associated with the stretching field. For the Burgers vortex, that component is not negligible for large z and has a global influence on the perturbations: as discussed above, it modifies the wavenumber of the perturbations according to $k \propto \exp(-\varepsilon^2 t)$. From an asymptotic point of view, this effect results from the condition of matching between the inner region $z \ll \varepsilon^{-2}$ dominated by the vortex and the outer region $z \gg \varepsilon^{-2}$ dominated by axial stretching. In terms of the slow variable $T = \varepsilon^2 t$, one can then write

$$k_B(T) = k_0 \mathrm{e}^{1-T}, \tag{4.3}$$

where k_0 is the dimensionless wavenumber at $T = 1$, or equivalently at $t = t_0 = R_\Gamma$.

For the Lamb–Oseen vortex, the dimensionless wavenumber k_L varies due the evolution of δ_L as

$$k_L(T) = k_0 T^{1/2}. \tag{4.4}$$

Let us then consider a perturbation to the basic flow (4.2*a–d*) with such evolving wavenumbers and write the total velocity and pressure field as

$$(U_r, U_\theta, U_z, \Pi) = (V_r, V_\theta, V_z, P) + (v_r, v_\theta, v_z, p)\mathrm{e}^{\mathrm{i}k(T)z}, \tag{4.5}$$

where $k(T)$ is given by (4.3) for the Burgers vortex and (4.4) for the Lamb–Oseen

vortex. For both vortices, the linearized equations obtained from the incompressible Navier–Stokes equation for the four-component vector $\boldsymbol{v} = (v_r, v_\theta, v_z, p)$ can be written in the form

$$\frac{\partial}{\partial t}(\boldsymbol{L}\boldsymbol{v}) + \boldsymbol{M}(k)\boldsymbol{v} = \varepsilon s^* \left(\mathrm{e}^{\mathrm{i}2\theta}\boldsymbol{N} + \mathrm{e}^{-\mathrm{i}2\theta}\overline{\boldsymbol{N}}\right)\boldsymbol{v}, \tag{4.6}$$

where $\boldsymbol{L}$, $\boldsymbol{M}(k)$ and $\boldsymbol{N}$ are the following operators (the primes denote differentiation with respect to r):

$$\boldsymbol{L} = \begin{pmatrix} 1 & 0 & 0 & 0 \\ 0 & 1 & 0 & 0 \\ 0 & 0 & 1 & 0 \\ 0 & 0 & 0 & 0 \end{pmatrix}, \tag{4.7a}$$

$$\boldsymbol{M}(k) = \begin{pmatrix} \Omega\dfrac{\partial}{\partial\theta} & -2\Omega & 0 & \dfrac{\partial}{\partial r} \\ 2\Omega + r\Omega' & \Omega\dfrac{\partial}{\partial\theta} & 0 & \dfrac{1}{r}\dfrac{\partial}{\partial\theta} \\ 0 & 0 & \Omega\dfrac{\partial}{\partial\theta} & \mathrm{i}k \\ \dfrac{\partial}{\partial r} + \dfrac{1}{r} & \dfrac{1}{r}\dfrac{\partial}{\partial\theta} & \mathrm{i}k & 0 \end{pmatrix}, \tag{4.7b}$$

$$\boldsymbol{N} = \begin{pmatrix} -\dfrac{F}{r}\dfrac{\partial}{\partial r} - \dfrac{F'}{r} + \dfrac{F}{r^2} - \mathrm{i}\dfrac{F'}{2r}\dfrac{\partial}{\partial\theta} & -\mathrm{i}\dfrac{2F}{r^2} + \mathrm{i}\dfrac{F'}{r} & 0 & 0 \\ -\mathrm{i}\dfrac{F'}{2} - \mathrm{i}\dfrac{F'}{2r} & -\dfrac{F}{r}\dfrac{\partial}{\partial r} + \dfrac{F'}{r} - \dfrac{F}{r^2} - \mathrm{i}\dfrac{F'}{2r}\dfrac{\partial}{\partial\theta} & 0 & 0 \\ 0 & 0 & -\dfrac{F}{r}\dfrac{\partial}{\partial r} - \mathrm{i}\dfrac{F'}{2r}\dfrac{\partial}{\partial\theta} & 0 \\ 0 & 0 & 0 & 0 \end{pmatrix}, \tag{4.7c}$$

$\Omega(r)$ denotes the azimuthal velocity divided by r:

$$\Omega(r) = \frac{1 - \mathrm{e}^{-r^2/4}}{2\pi r^2}, \tag{4.8}$$

and $\overline{\boldsymbol{N}}$ is the matrix whose elements are the complex conjugates of those in $\boldsymbol{N}$.

As explained in the previous section, the perturbation $\boldsymbol{v}$ is assumed to be, at leading order, a combination of resonant stationary helical Kelvin waves of azimuthal wavenumbers $m = \pm 1$

$$\boldsymbol{v}^{\pm} = \Phi^{\pm}(r)\exp(\mathrm{i}\kappa z \pm \mathrm{i}\theta). \tag{4.9}$$

These waves satisfy an equation which is obtained by neglecting the right-hand side of (4.6) and the time-variation of k:

$$\boldsymbol{M}(\kappa)\left(\Phi^{\pm}\mathrm{e}^{\pm\mathrm{i}\theta}\right) = 0, \tag{4.10}$$

where $\Phi^{\pm}$ is finite at zero and vanishes at $+\infty$. These boundary conditions select 'vortex modes', that is perturbations which are localized in the neighbourhood of the vortex core and potential for large r. This latter property guarantees that, as in Tsai & Widnall (1976), the vortex modes are not influenced by the outer region dominated by the potential strain field. System (4.10) can be reduced to a boundary

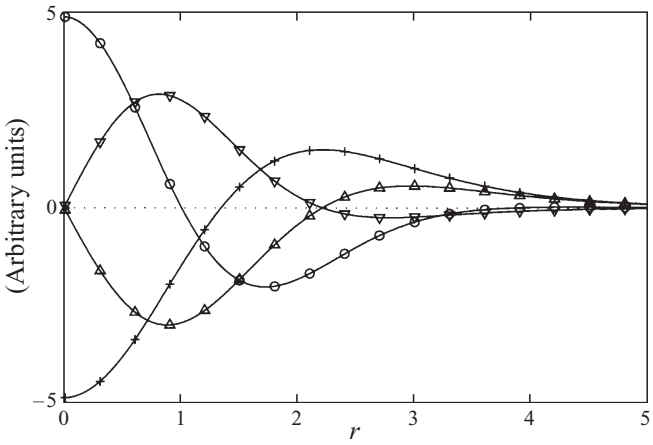

FIGURE 3. Four components of the eigenvector $\Phi^+(r) = (\mathrm{i}u_r, u_\theta, u_z, p)$ for $\kappa = 1.13$: $+$, u_r; $\bigcirc$, u_θ; $\triangle$, u_z; $\triangledown$, $30 \times p$.

value problem for the pressure (see Moore & Saffman 1975 and Saffman 1992) which gives after numerical integration the resonant wavenumbers κ and their corresponding eigenmodes:

$$\Phi^{\pm} = (\pm \mathrm{i}u_r, u_\theta, \pm u_z, p), \tag{4.11}$$

where u_r, u_θ, u_z and p are real functions of r. Figure 3 shows the components of Φ^+ for the smallest non-zero resonant wavenumber $\kappa \approx 1.13$. Larger resonant wavenumbers are given in table 1 below.

According to the above discussion, the helical modes are resonant during a finite period of time of order $sR_\Gamma \delta^4/\Gamma^2$, i.e. of order ε^{-1} with the scaling (4.1). This time scale is slow compared to the $O(1)$ vorticity time scale but fast compared to the $O(\varepsilon^{-2})$ evolution scale of k. The description of the resonance phenomenon in the limit of small ε then requires the introduction of a new intermediate time variable

$$\overline{T} = \frac{T-1}{\varepsilon} = \varepsilon(t - t_0). \tag{4.12}$$

In equation (4.6), time-dependency only appears through the operator $\boldsymbol{M}$. The transient effect occurring on the intermediate time scale $\overline{T} = O(1)$ is then taken into account by expanding $\boldsymbol{M}$ in Taylor series with respect to the small parameter ε

$$\boldsymbol{M}(k) = \boldsymbol{M}(\kappa) + \mathrm{i}\varepsilon\overline{T} \left.\frac{\mathrm{d}k}{\mathrm{d}T}\right|_{T=1} \boldsymbol{Q} + O(\varepsilon^2), \tag{4.13}$$

where

$$\boldsymbol{Q} = \begin{pmatrix} 0 & 0 & 0 & 0 \\ 0 & 0 & 0 & 0 \\ 0 & 0 & 0 & 1 \\ 0 & 0 & 1 & 0 \end{pmatrix}. \tag{4.14}$$

The derivative $\mathrm{d}k/\mathrm{d}T$ is obtained from (4.3) and (4.4):

$$\left.\frac{\mathrm{d}k}{\mathrm{d}T}\right|_{k_0=1,\, T=1} = \xi\kappa, \tag{4.15}$$

with $\xi = \xi_L = \frac{1}{2}$ for the Lamb–Oseen vortex and $\xi = \xi_B = -1$ for the Burgers vortex.

Following classical asymptotic methods (see for instance Van Dyke 1975), perturbations are also expanded in terms of ε as

$$\boldsymbol{v} = \boldsymbol{v}_0(\overline{T}, \theta, r) + \varepsilon \boldsymbol{v}_1(\overline{T}, \theta, r) + \varepsilon^2 \boldsymbol{v}_2 + \cdots, \tag{4.16}$$

where the leading-order term $\boldsymbol{v}_0$ is a combination of the resonant waves multiplied by a slowly varying amplitude:

$$\boldsymbol{v}_0 = A^+(\overline{T})\mathrm{e}^{\mathrm{i}\theta}\boldsymbol{\Phi}^+(r) + A^-(\overline{T})\mathrm{e}^{-\mathrm{i}\theta}\boldsymbol{\Phi}^-(r). \tag{4.17}$$

Upon rewriting equation (4.6) with (4.13) for $\boldsymbol{M}$ and (4.16) for $\boldsymbol{v}$, one obtains an equation for $\boldsymbol{v}$ up to $O(\varepsilon^2)$ terms. The above choice for $\boldsymbol{v}_0$ guarantees that $O(1)$ terms vanish. Cancelling terms at the order ε leads to the following equation for $\boldsymbol{v}_1$:

$$\frac{\partial}{\partial t}\boldsymbol{L}\boldsymbol{v}_1 + \boldsymbol{M}(\kappa)\boldsymbol{v}_1 = -\frac{\partial}{\partial \overline{T}}\boldsymbol{L}\boldsymbol{v}_0 - \mathrm{i}\xi\kappa\boldsymbol{Q}\overline{T}\boldsymbol{v}_0 + s^*\left(\mathrm{e}^{\mathrm{i}2\theta}\boldsymbol{N} + \mathrm{e}^{-\mathrm{i}2\theta}\overline{\boldsymbol{N}}\right)\boldsymbol{v}_0. \tag{4.18}$$

This equation is solved by taking $\boldsymbol{v}_1$ of the form

$$\boldsymbol{v}_1 = \boldsymbol{v}_1^+(\overline{T}, r)\mathrm{e}^{\mathrm{i}\theta} + \boldsymbol{v}_1^-(\overline{T}, r)\mathrm{e}^{-\mathrm{i}\theta} + \boldsymbol{w}_1^+(\overline{T}, r)\mathrm{e}^{3\mathrm{i}\theta} + \boldsymbol{w}_1^-(\overline{T}, r)\mathrm{e}^{-3\mathrm{i}\theta}. \tag{4.19}$$

Such a choice gives for $\boldsymbol{v}_1^+$ and $\boldsymbol{v}_1^-$

$$\boldsymbol{M}^+(\kappa)\boldsymbol{v}_1^+ = -\frac{\partial A^+}{\partial \overline{T}}\boldsymbol{L}\boldsymbol{\Phi}^+ - \mathrm{i}\xi\kappa\overline{T}A^+\boldsymbol{Q}\boldsymbol{\Phi}^+ + s^*A^-\boldsymbol{N}\boldsymbol{\Phi}^-, \tag{4.20a}$$

$$\boldsymbol{M}^-(\kappa)\boldsymbol{v}_1^- = -\frac{\partial A^-}{\partial \overline{T}}\boldsymbol{L}\boldsymbol{\Phi}^- - \mathrm{i}\xi\kappa\overline{T}A^-\boldsymbol{Q}\boldsymbol{\Phi}^- + s^*A^+\overline{\boldsymbol{N}}\boldsymbol{\Phi}^+, \tag{4.20b}$$

where $\boldsymbol{M}^\pm$ denotes the operator $\boldsymbol{M}$, where $\partial/\partial\theta$ is replaced by $\pm\mathrm{i}$.

The condition of solvability of these non-homogeneous equations requires that the forcing term (right-hand side) of each equation is orthogonal to the adjoint mode of the homogeneous operator (left-hand side). For each operator $\boldsymbol{M}^\pm(\kappa)$, the adjoint mode satisfies

$$\boldsymbol{M}_A^\pm(\kappa)\boldsymbol{\Phi}_A^\pm = 0, \tag{4.21}$$

where $\boldsymbol{M}_A^\pm(\kappa)$ is defined by $\langle \boldsymbol{X}|\boldsymbol{M}^\pm(\kappa)\boldsymbol{Y}\rangle = \overline{\langle \boldsymbol{M}_A^\pm(\kappa)\boldsymbol{X}|\boldsymbol{Y}\rangle}$ with the following scalar product:

$$\langle \boldsymbol{X}|\boldsymbol{Y}\rangle = \int_0^\infty \left(\overline{X}_1Y_1 + \overline{X}_2Y_2 + \overline{X}_3Y_3 + \overline{X}_4Y_4\right)\mathrm{d}r. \tag{4.22}$$

Equation (4.21) is similar to (4.10) and its integration can be carried out with the same numerical method. In particular, the adjoint modes $\boldsymbol{\Phi}_A^\pm$ are found to satisfy the same symmetry property (4.11) as $\boldsymbol{\Phi}^\pm$. As a result, the solvability conditions for (4.20) reads

$$L^{++}\frac{\partial A^+}{\partial \overline{T}} + \mathrm{i}\xi\kappa Q^{++}\overline{T}A^+ - s^*N^{+-}A^- = 0, \tag{4.23a}$$

$$L^{--}\frac{\partial A^-}{\partial \overline{T}} + \mathrm{i}\xi\kappa Q^{--}\overline{T}A^- - s^*\overline{N}^{-+}A^+ = 0, \tag{4.23b}$$

where the notation N^{+-} stands for $\langle \boldsymbol{\Phi}_A^+|\boldsymbol{N}\boldsymbol{\Phi}^-\rangle$. The symmetry property (4.11) yields

κ	$q \times 10^3$	$q\kappa \times 10^3$	n	$s^*_{cBurgers}$	s^*_{cLamb}
1.13	11.3	12.8	0.6895	0.1304	0.0924
1.97	6.86	13.5	0.6944	0.1331	0.0946
2.80	4.91	13.7	0.6957	0.1340	0.0952
3.63	3.82	13.9	0.6961	0.1350	0.0954
4.44	3.12	13.9	0.6957	0.1350	0.0954

TABLE 1. Different values of the computed scalar products q and n (defined in the text in (4.24a–c)) and $s^*_c = (|2q\xi\kappa|/\pi n^2)^{1/2}$ for the first five κ.

the following relations between the coefficients:

$$L^{++} = L^{--}, \tag{4.24a}$$

$$\frac{Q^{--}}{L^{++}} = -\frac{Q^{++}}{L^{++}} = q, \tag{4.24b}$$

$$\frac{N^{+-}}{L^{++}} = \frac{\overline{N}^{-+}}{L^{++}} = n, \tag{4.24c}$$

where q and n are real numbers. Equations (4.23a, b) become

$$\frac{\partial A^+}{\partial \overline{T}} - \mathrm{i}q\xi\kappa\overline{T}A^+ - s^*nA^- = 0, \tag{4.25a}$$

$$\frac{\partial A^-}{\partial \overline{T}} + \mathrm{i}q\xi\kappa\overline{T}A^- - s^*nA^+ = 0. \tag{4.25b}$$

The coefficients q and n are the same for both vortices but ξ has a different value for each vortex ($\xi_B = -1$ and $\xi_L = 1/2$). Numerical values for each resonant wavenumber κ are given in table 1.

The amplitude equations (4.25a, b) can be reduced to a single equation

$$\frac{\partial^2 A^\pm}{\partial \overline{T}^2} + \left(\mp \mathrm{i}q\xi\kappa + (q\xi\kappa\overline{T})^2 - (s^*n)^2\right) A^\pm = 0, \tag{4.26}$$

which is easily solved in term of parabolic cylinder functions $\boldsymbol{D}_\mu$ (see Bender & Orszag 1978) as

$$A^\pm(\overline{T}) = a_1^\pm \boldsymbol{D}_{\mp \mathrm{i}\mu}(\eta \mathrm{e}^{\mp sgn(\xi)\mathrm{i}\pi/4}\overline{T}) + a_2^\pm \boldsymbol{D}_{\mp \mathrm{i}\mu}(-\eta \mathrm{e}^{\mp sgn(\xi)\mathrm{i}\pi/4}\overline{T}), \tag{4.27}$$

with

$$\mu = \frac{(s^*n)^2}{2q\xi\kappa}, \tag{4.28a}$$

$$\eta = |2q\xi\kappa|^{1/2}. \tag{4.28b}$$

Using (4.25a, b) at $\overline{T} = 0$, the following relation between the coefficients $a_1^\pm$ and $a_2^\pm$ can be deduced:

$$\frac{a_1^\pm - a_2^\pm}{a_1^\mp + a_2^\mp} = K^\pm = \frac{-s^*n}{\sqrt{2}\eta \mathrm{e}^{\mp sgn(\xi)\mathrm{i}\pi/4}} \frac{\Gamma\left(\pm\frac{1}{2}\mathrm{i}\mu\right)}{\Gamma\left(\frac{1}{2} \pm \frac{1}{2}\mathrm{i}\mu\right)}, \tag{4.29}$$

where $\Gamma(x)$ stands for the usual Gamma function.

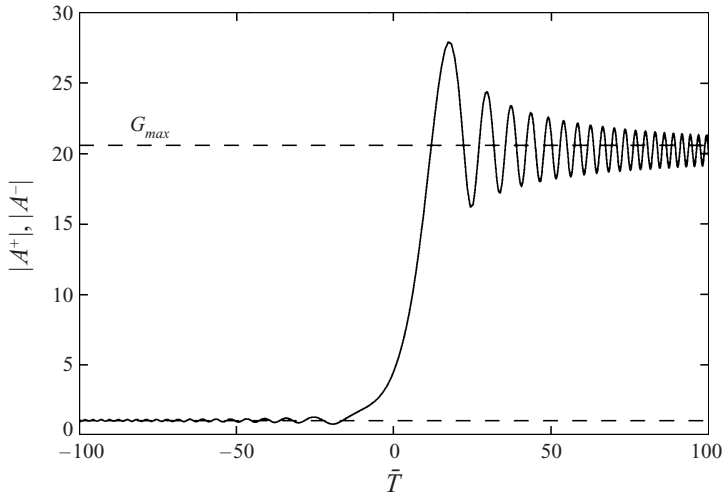

FIGURE 4. Typical temporal behaviour of the perturbation amplitude $|A^{\pm}|$. The graph shows the time evolution of $|A^{\pm}|$ with the initial conditions (at $\overline{T} = -100$): $A^+ = \mathrm{i}$, $A^- = -\mathrm{i}$ (in this case, A^+ and A^- remain complex conjugates) for the smallest resonant wavenumber $\kappa \approx 1.13$ and $s^* = 0.2$ in the case of the Burgers vortex. The gain of the amplitude G is close to $G_{max} \approx 20.6$.

The behaviour of $A^{\pm}$ given by expression (4.27) has already been analysed in Le Dizès *et al.* (1996). For small $|\overline{T}|$, $A^{\pm}$ grows as $A^{\pm}(\overline{T}) \propto \exp\left(s^* n \overline{T}\right)$ whereas $A^{\pm}$ has, for large $|\overline{T}|$, an oscillating behaviour of the form

$$A^{\pm}(\overline{T}) \underset{\overline{T}\to-\infty}{\sim} A^{\pm}_{-\infty} \left(\eta|\overline{T}|\right)^{\mp \mathrm{i}\mu} \exp\left(\pm \mathrm{i}(\eta\overline{T})^2/4\right), \tag{4.30a}$$

$$A^{\pm}(\overline{T}) \underset{\overline{T}\to+\infty}{\sim} A^{\pm}_{+\infty} \left(\eta|\overline{T}|\right)^{\mp \mathrm{i}\mu} \exp\left(\pm \mathrm{i}(\eta\overline{T})^2/4\right), \tag{4.30b}$$

where $A^{\pm}_{-\infty}$ and $A^{\pm}_{+\infty}$ are amplitude factors at $\overline{T} = -\infty$ and $\overline{T} = +\infty$ respectively. A typical evolution for $A^{\pm}$ is shown on figure 4. Using the asymptotic expansions of the parabolic functions and expression (4.29), both amplitude factors can be related through the expression

$$A^{\pm}_{+\infty} = \frac{2B^{\pm}A^{\mp}_{-\infty} - (B^+B^- + 1)A^{\pm}_{-\infty}}{B^+B^- - 1}, \tag{4.31}$$

where $B^{\pm} = K^{\pm}\tanh(\frac{1}{2}sgn(\xi)\pi\mu)$ and $|B^{\pm}|^2 = B^+B^- = \tanh(\frac{1}{2}\pi|\mu|)$. This expression shows that the helical wave amplitudes, before and after the resonance, are connected. The gain of amplitude across the region of resonance can be defined by the quantity

$$G = \left(\frac{|A^+_{+\infty}|^2 + |A^-_{+\infty}|^2}{|A^+_{-\infty}|^2 + |A^-_{-\infty}|^2}\right)^{1/2}. \tag{4.32}$$

This gain is calculated exactly as

$$G^2 = g_1 + g_2 \frac{a + \overline{a}}{1 + |a|^2}, \tag{4.33}$$

where

$$g_1 = \frac{|B^+B^- + 1|^2 + 4|B^{\pm}|^2}{|B^+B^- - 1|^2} = 1 + 8\sinh\frac{\pi|\mu|}{2}\cosh\frac{\pi|\mu|}{2}\mathrm{e}^{\pi|\mu|}, \tag{4.34a}$$

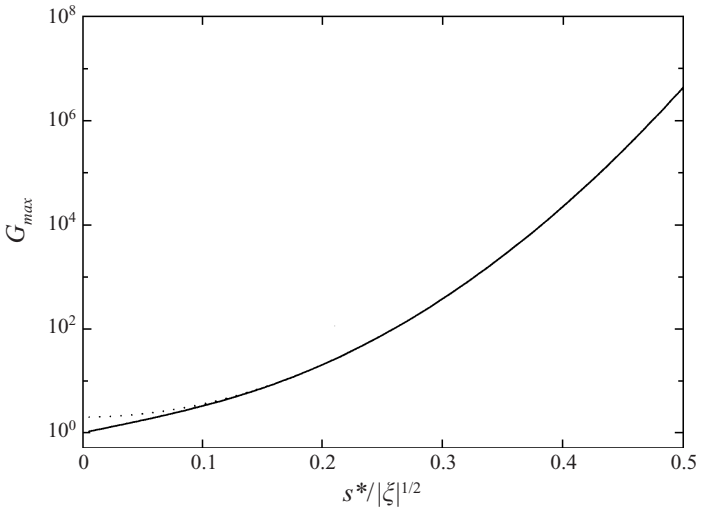

FIGURE 5. Plot of the maximum gain G_{max} as a function of $s^*/|\xi|^{1/2}$ for the smallest resonant wavenumber $\kappa \approx 1.13$. Solid line: $G_{max} = (g_1 + g_2)^{1/2}$, dotted line: $2\exp(s^*/s_c^*)^2$.

$$g_2 = 4|B^+|\frac{B^+B^- + 1}{|B^+B^- - 1|^2} = 4\left(\tanh\frac{\pi|\mu|}{2}\right)^{1/2}\cosh\frac{\pi|\mu|}{2}e^{3\pi|\mu|/2}, \tag{4.34b}$$

$$a = \frac{B^+A^-_{-\infty}}{|B^+|A^+_{-\infty}}. \tag{4.34c}$$

The gain G depends on the helical wave decomposition before the resonance. This dependence appears through the coefficient a which can take any value in the complex plane according to the relative amplitude and phase of the two waves before the resonance. This leads to the inequality $g_1 - g_2 \leqslant G^2 \leqslant g_1 + g_2$ where the maximum value $G_{max} = (g_1 + g_2)^{1/2}$ is reached for $a = 1$. In the limit $e^{\pi|\mu|} \gg 1$, G_{max} reduces to a simple expression

$$G_{max} \sim 2e^{\pi|\mu|} = 2e^{(s^*/s_c^*)^2}, \tag{4.35}$$

where

$$s_c^{*2} = \frac{|2q\xi\kappa|}{\pi n^2}. \tag{4.36}$$

The values of s_c^* for each vortex and each resonant wavenumber are given in table 1. The behaviour of G_{max} as a function of $s^*/|\xi|^{1/2}$ is displayed on figure 5.

This figure constitutes an important result of the paper. Using $|\xi_B| = 1$ and $|\xi_L| = 1/2$, it gives the maximum gain G_{max} of the helical modes for the Burgers and Lamb–Oseen vortices in a strain field. Assuming that $G_{max} > 10^4$ is sufficient to destabilize the vortex, it then provides an explicit criterion of 'instability' which is $s^* \gtrsim 0.4$ for the Burgers vortex, and $s^* \gtrsim 0.3$ for the Lamb–Oseen vortex. Figure 5 will also be used in the next section to determine the instability properties of an arbitrarily stretched vortex.

5. Instability characteristics

In the first part of this section, the dependence of the instability characteristics on the strain rate is analysed. In particular, it is argued that the strain rate in the

	Rankine		Gaussian		
	κ_1	κ_2	κ_1	κ_2	Elliptical
κ	2.50	4.35	1.13	1.97	—
σ/s_∞	1.1416	1.1390	1.3790	1.3888	0.5625
σ/s_0	0.5708	0.5694	0.5462	0.5500	0.5625

TABLE 2. Growth rate σ of the TWMS instability for the Rankine vortex, the Gaussian vortex and the pure elliptical flow for the first two resonant wavenumbers κ according to the strain rate at $r = \infty$ and $r = 0$ (s_∞ and s_0 respectively).

vortex core could be the main parameter governing the transient growth rate of the instability. The effect of the vorticity profile on that parameter is also addressed using a simple example. In the second part, we focus on the role of stretching in the instability process. The present study is generalized to Gaussian vortices in an arbitrary time-dependent stretching field.

5.1. *Dependence on the strain rate*

The coefficient n in (4.23a, b) measures the strength of the instability. Without stretching or viscous effects, the growth rate of the helical waves is (written in a dimensional form)

$$\sigma = 2ns. \tag{5.1}$$

This quantity corresponds to the growth rate of the TWMS instability in the case of a Gaussian vorticity profile. In table 2, this growth rate is compared to the values obtained for the Rankine vortex for the two smallest non-zero wavenumbers (Tsai & Widnall 1976). The growth rate is normalized by the strain rate at infinity in the third row, and by the strain rate in the vortex centre in the last row. It is important to point out that growth rates are very similar when normalized with the strain rate in the vortex centre and very close to the value $\sigma_E/s = \frac{9}{16} = 0.5625$ obtained for a pure elliptical flow (Waleffe 1990). This emphasizes the intimate link between the TWMS instability and the elliptical instability already mentioned in the introduction. This result was expected for large wavenumbers because of the localization near the vortex centre of such modes. However, in the present case, it is surprising to observe so small a correction with respect to the elliptical instability characteristics as the unstable modes spread over a fairly large region (see figure 3). Based on the results for the Rankine and Gaussian vortices, it is natural to conjecture that for other vorticity profiles a good estimate for the TWMS instability growth rate is given by the growth rate of the elliptical instability of the centre, i.e. $\sigma = \frac{9}{16}s_0$ where s_0 is the vortex-centre strain rate.

The nature of the vorticity profile has an indirect effect on the TWMS instability growth rate as it modifies the ratio s_0 between the external strain rate at infinity and the strain rate in the vortex centre. In particular, this ratio is 2 for a Rankine vortex while it is $s_0 \approx 2.525$ for the Gaussian vortex. One could then naturally address the question whether there exists a vorticity profile that maximizes this ratio, and which, consequently could maximize the growth rate. This issue is now addressed for a simple class of vortices: the generalized Rankine vortices whose vorticity distribution is given on figure 6. These vortices are characterized by the relative size of the 'band' around the vortex core, i.e. by its width $b - 1$, ($b > 1$) and its strength a. After a long but

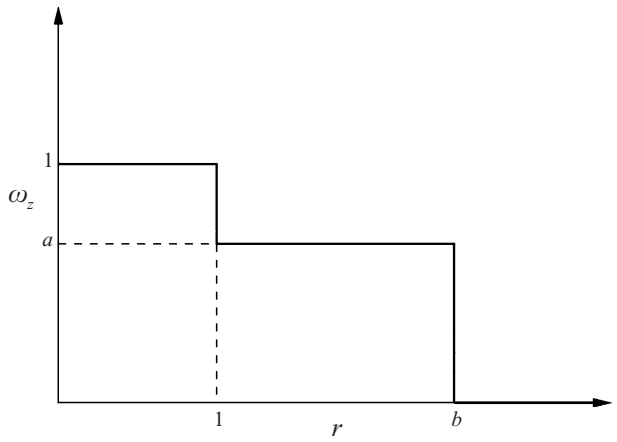

FIGURE 6. Vorticity distribution of the generalized Rankine vortex.

straightforward calculation, an expression for s_0 is obtained as

$$s_0 = \frac{2b^2(1 + a(b^2 - 1))}{b^2 + \frac{1}{2}a(b^4 - 1) + \frac{1}{2}a^2(b^2 - 1)^2}. \tag{5.2}$$

If one allows negative a, this expression has no upper limit. Thus, the strain in the vortex centre is *a priori* as large as wanted. However, vortices with $a < 0$ are unstable with respect to centrifugal instability since $(rV_\theta(r))^2$ is no longer an increasing function (Rayleigh criterion) in such a case. If one only considers centrifugally stable vortices, s_0 reaches a maximum value $s_{0max} = 4$ in the limit of large circulation and small strength ($b^2 a \gg 1$ with $a \ll 1$). Although this value is finite, it is nevertheless larger than the one obtained for the vortices mentioned above.

5.2. *Dependence on the stretching rate*

For both Burgers and Lamb–Oseen vortices, the TWMS instability has been shown to be transient due to the time variation of the product $k\delta$. This effect is expressed in the parameter ξ appearing in expression (4.36) for s_c^{*2}. The modulus of this parameter actually gives the evolution time scale of the product $k\delta$ at the moment of resonance. It can be written with dimensional quantities as

$$\xi = \frac{\delta_0^2}{\nu}\left[\frac{1}{k\delta}\frac{\mathrm{d}k\delta}{\mathrm{d}t}\right]_{k_0\delta_0=\kappa,t=0}, \tag{5.3}$$

where δ_0 and k_0 are the initial values of radius and wavenumber at resonance. Time variations are directly connected to the stretching field applied to the vortex. They can be calculated for any time-varying stretching field $\boldsymbol{U}_\gamma = (-\frac{1}{2}\gamma(t)x, -\frac{1}{2}\gamma(t)y, \gamma(t)z)$ as follows. The evolution of the axial wavenumber is governed by (3.2). Its general solution is

$$k(t) = \frac{k_0}{S(t)}, \tag{5.4}$$

where

$$S(t) = \exp\left(\int_0^t \gamma(u)\mathrm{d}u\right). \tag{5.5}$$

The variation of the radius can be obtained from the Lundgren transform (Lundgren 1982). This transform gives the vorticity field of any two-dimensional solution subjected to an arbitrary perpendicular stretching field. For a time-varying stretching rate $\gamma(t)$, the vortex is then still given by (2.3) and (2.6*a–d*) but its radius now evolves according to

$$\delta^2 = \frac{\delta_0^2 + \nu \int_0^t S(u)\mathrm{d}u}{S(t)}. \tag{5.6}$$

It follows that, in the general case,

$$k\delta = \frac{k_0}{(S(t))^{\frac{3}{2}}} \left(\delta_0^2 + \nu \int_0^t S(u)\mathrm{d}u\right)^{1/2}. \tag{5.7}$$

Expression (5.3) for ξ then becomes

$$\xi = -\tfrac{3}{2}\left(\gamma^* - \tfrac{1}{3}\right), \tag{5.8}$$

where γ^* is the dimensionless stretching rate at resonance:

$$\gamma^* = \frac{\gamma_0 \delta_0^2}{\nu}. \tag{5.9}$$

Expression (5.8) shows the effect of the stretching rate on the stability properties of the vortex. Indeed, as $|\xi|$ decreases, the gain increases, and consequently the vortex becomes more unstable. It confers on stretching a non-trivial role: increasing the stretching rate is destabilizing for the Lamb–Oseen vortex but stabilizing for the Burgers vortex. Moreover, it is worth noting that for given radius and circulation, the Lamb–Oseen vortex is more unstable than the Burgers vortex.

The most unstable vortex corresponds to a configuration for which $\gamma^* = \frac{1}{3}$. For this value, the maximum gain G_{max} computed above becomes infinite which shows that the present analysis no longer applies. This is actually due to the vanishing of the time-dependent term in the amplitude equations (4.25*a, b*) which should be replaced by the first non-zero term in the Taylor expansion of $k\delta$. Both the scaling and the amplitude equation are therefore modified in such a case but a similar analysis can be carried out to compute the exact gain G_{max}. All the time-dependent terms of the Taylor expansion can even be zero, if $k\delta$ remains constant. This occurs for the particular time-dependent stretching rate

$$\gamma(t) = \frac{1}{2t + 3\delta_0^2/\nu}, \tag{5.10}$$

which is obtained by solving the differential equation deduced from (5.7). If one agrees with the analysis of §3, this last case should be the most unstable configuration since $k\delta$ does not leave the unstable band around the resonant wavenumber (see figure 2*a, b*). One then expects the amplitude of the perturbation to evolve at leading order according to $A^{\pm} \propto \exp(2nst)$ as long as second-order effects are negligible, which means instability if $s^* \gg 1/R_\Gamma^{1/2}$.

6. Discussion

In this paper, we have studied the linear stability of a family of stretched vortices including the Burgers and Lamb–Oseen vortices subjected to a perpendicular strain field in the limit of large Reynolds numbers R_Γ, small strain and small stretching. The

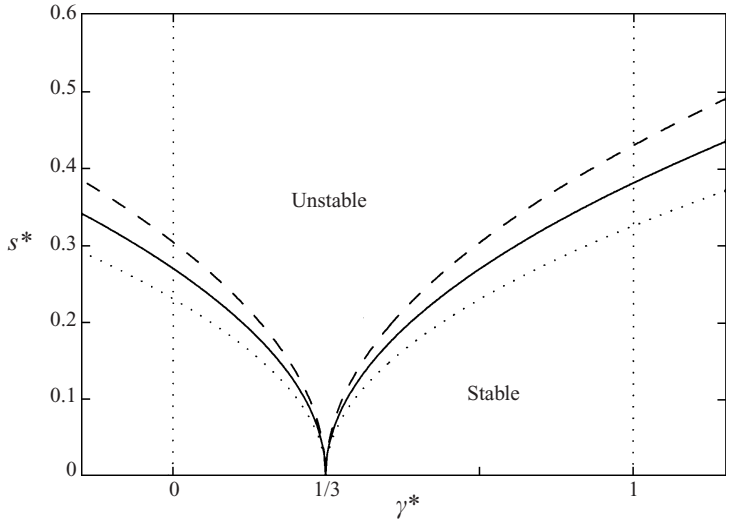

FIGURE 7. Level curves of the maximum gain G_{max} in the (γ^*, s^*)-plane. The Burgers and Lamb–Oseen vortices correspond to $\gamma^* = 1$ and $\gamma^* = 0$ respectively. Dotted line: $G_{max} = 10^3$, solid line: $G_{max} = 10^4$, dashed line: $G_{max} = 10^5$.

destabilization by the resonance mechanism described by Tsai & Widnall (1976) and Moore & Saffman (1975) has been considered and generalized to take into account viscous and stretching effects. The main modification has been the introduction of a transient aspect in the instability mechanism which has been related to the time evolution of the dimensionless axial wavenumber $k\delta$ of the resonant helical waves.

The instability properties have been connected to the values of two dimensionless parameters: $s^* = 2s\delta^2 R_\Gamma^{1/2}/\Gamma$ and $\gamma^* = \gamma\delta^2/\nu$, where s is the perpendicular strain rate, γ the stretching rate, δ the vortex radius and Γ the circulation. The Burgers and Lamb–Oseen vortices are two particular cases associated with the values $\gamma^* = 1$ and $\gamma^* = 0$ respectively. The maximum gain of amplitude of the helical waves has been computed. The result is summarized on figure 7 which displays the level curves of the maximum gain in the (γ^*, s^*)-plane. This graph characterizes the sensitivity of the vortex to the resonance mechanism. In particular, if the vortex parameters (γ^*, s^*) correspond to a point above the solid curve in figure 7, the amplitude gain of the resonant waves is larger than 10^4. In such a case, the sensitivity is so important that one expects the vortex not to survive. For the Burgers vortex, this condition reduces to $s/\gamma > 0.2R_\Gamma^{1/2}$, which means that only strong biaxial configurations are destabilized by resonance. For the particular stretching parameter $\gamma^* = \frac{1}{3}$, the gain is exponentially large (as $R_\Gamma \to \infty$) for all $s^* = O(1)$. For a fixed $s^* \neq 0$, the most unstable vortex is then always obtained as $\gamma^* \to \frac{1}{3}$. Note however that the vortices are linearly stable with respect to infinitesimal perturbations since the gain is always finite.

The influence of the vorticity profile on the instability characteristics has also been studied. We have noticed that the growth rate of TWMS instability for both Rankine and Gaussian vortices is well approximated by the growth rate associated with the elliptical instability of its core, i.e. $\sigma \approx \frac{9}{16}s_0$ where s_0 is the perpendicular strain rate in the vortex centre. But, we have shown that the ratio of this local strain rate to the external strain rate depends on the vorticity profile and can even reach arbitrarily large values for particular cases.

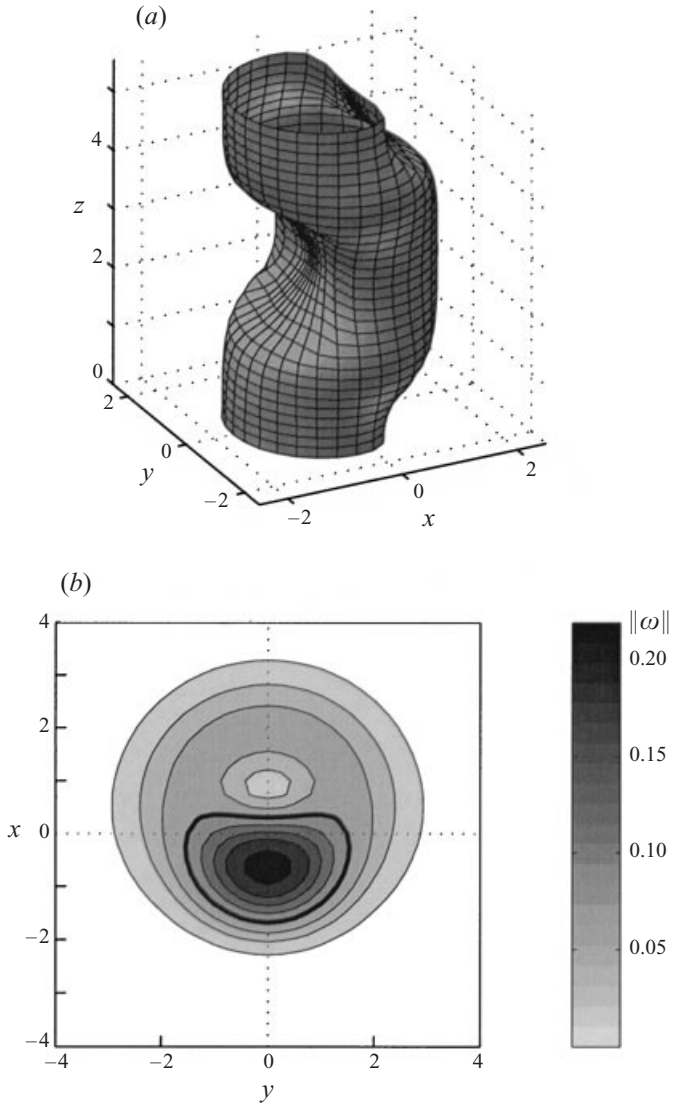

FIGURE 8. Contour plot of the magnitude of the dimensionless vorticity where the perturbation is such that $A^+ = A^-$ and $v_\theta/V_\theta = 0.4$ in $r = 0$. (*a*) Three-dimensional representation for $\|\omega\| = 0.09$. (*b*) Contour plots in the plane $z = 0$, the bold line represents the contour $\|\omega\| = 0.09$.

The unstable mode is formed of two helical waves of azimuthal wavenumber $m = -1$ and $m = 1$. There is *a priori* a discrete infinity of unstable axial wavenumbers. But if viscous effects on the perturbation are considered (these effects are negligible in the asymptotic analysis of §4), one expects the smallest non-zero wavenumber to be selected. The basic vortex plus the unstable mode are displayed on figure 8. Note that the two helices associated with the two helical modes compensate to form a sinuous deformation of the vortex filament.

A large part of the paper was focused on the analysis of the transient growth of the resonant helical waves. Amplitude equations (4.25*a, b*), which fully describe the complex interactions of these waves in time, have been derived. They can be

generalized to account for slow axial variation along the vortex by introducing a dependence of the perturbation on the slow variable $\overline{Z} = z/\varepsilon$ (see e.g. Moore & Saffman 1975). The resulting equations are

$$\frac{\partial A^+}{\partial \overline{T}} - q\frac{\partial A^+}{\partial \overline{Z}} - \mathrm{i}q\xi\kappa\overline{T}A^+ - s^*nA^- = 0, \tag{6.1a}$$

$$\frac{\partial A^-}{\partial \overline{T}} + q\frac{\partial A^-}{\partial \overline{Z}} + \mathrm{i}q\xi\kappa\overline{T}A^- - s^*nA^+ = 0. \tag{6.1b}$$

These equations allow a description of the destabilization process in the case of localized perturbations as well as in a geometry confined in the z-direction. They also show that a small change in the axial wavenumber can be treated as a mere time shift.

In this paper, we have considered a particular perturbation composed of helical modes with azimuthal wavenumber $m = \pm 1$ but the present study can be easily applied to other combinations of modes. Basically any combination of two waves having the same frequency, the same axial wavenumber, and azimuthal wavenumbers differing by 2 constitutes a configuration which resonates with the strain field. For a bounded elliptical vortex with uniform vorticity, Waleffe (1989) showed that the maximum growth rate of such combinations depends slightly on their azimuthal wavenumber. This growth rate similarity could explain the rich dynamical behaviour of vortices in experiments and numerical simulations of high-Reynolds-number flows (Cadot *et al.* 1995; Arendt *et al.* 1998). Indeed, a combination of modes $m = 0$ and $m = 2$ could account for the spliting of vortices while modes $m = 1$ and $m = 3$ could be responsible for the formation of strands. However, for low-Reynolds-number flows, viscosity is expected to strongly filter large azimuthal wavenumbers as well as large axial wavenumbers. This may explain why only helical modes were observed in several experiments (for instance, Leweke & Williamson 1998*a* and Gledzer & Ponomarev 1992).

Nevertheless, an improved understanding of the complex behaviour of vortices observed in experiments probably requires the introduction of nonlinearities in the present analysis. Very few results have been obtained so far. Waleffe (1989) considered weakly nonlinear effects in the case of bounded elliptical flows. He showed that nonlinearity tends to detune the axial wavenumbers of the resonant modes, and to generate a rotation of the perturbation around the vortex axis, in agreement with the local induction approximation for plane slender vortices (see Saffman 1992). Lifschitz & Fabijonas (1996) and Fabijonas, Holm & Lifschitz (1997) studied the secondary instability of unbounded circular and elliptical flows respectively. They obtained the surprising result that the uniform basic flow plus an inertial wave could become unstable with an unbounded growth rate. It would be very interesting to extend their theory to the present framework. This could indeed give an alternative explanation for the bursting of vortex filaments. We also pointed out above that vortices are also subject to the tilting instability when they are placed in a strong biaxial strain field. It would be interesting to analyse this instability in detail to fully understand its role in real experimental configuration.

This work has benefitted from discussions with M. Rossi. We kindly thank him for his interest and encouragement.

REFERENCES

Arendt, S., Fritts, D. C. & Andreassen, Ø. 1998 Kelvin twist waves in the transition to turbulence. *Eur. J. Mech.* B/*Fluids* **17**, 595–604.

Ash, R. L. & Khorrami, M. R. 1995 Vortex stability. In *Fluid Vortices* (ed. S. I. Green), Chap. VIII, pp. 317–372. Kluwer.

Bayly, B. J. 1986 Three-dimensional instability of elliptical flow. *Phys. Rev. Lett.* **57**, 2160–2163.

Bayly, B. J., Holm, D. D. & Lifschitz, A. 1996 Three-dimensional stability of elliptical vortex columns in external strain flows. *Phil. Trans. R. Soc. Lond.* A **354**, 895–926.

Bender, C. M. & Orszag, S. A. 1978 *Advanced Mathematical Methods for Scientists and Engineers.* McGraw-Hill.

Bernoff, A. J. & Lingevitch, J. F. 1994 Rapid relaxation of an axisymmetric vortex. *Phys. Fluids* **6**, 3717–3723.

Cadot, O., Douady, S. & Couder, Y. 1995 Characterization of the low pressure filaments in three-dimensional turbulent shear flow. *Phys. Fluids* **7**, 630–646.

Cambon, C., Benoit, J.-P., Shao, L. & Jacquin, L. 1994 Stability analysis and large-eddy simulation of rotating turbulence with organized eddies. *J. Fluid Mech.* **278**, 175–200.

Craik, A. D. D. 1989 The stability of unbounded two- and three-dimensional flows subject to body forces: some exact solutions. *J. Fluid Mech.* **198**, 275–292.

Craik, A. D. D. & Criminale, W. O. 1986 Evolution of wavelike disturbances in shear flows: a class of exact solutions of the Navier-Stokes equations. *Proc. R. Soc. Lond.* A **406**, 13–26.

Escudier, M. P. 1984 Observations of the flow produced in a cylinder container by a rotating endwall. *Exps. Fluids* **2**, 189–196.

Fabijonas, B., Holm, D. D. & Lifschitz, A. 1997 Secondary instabilities of flows with elliptical streamlines. *Phys. Rev. Lett.* **78**, 1900–1903.

Foster, G. K. & Craik, A. D. D. 1996 The stability of three-dimensional time-periodic flows with ellipsoidal stream surfaces. *J. Fluid Mech.* **324**, 379–391.

Gledzer, E. B. & Ponomarev, V. M. 1992 Instability of bounded flows with elliptical streamlines. *J. Fluid Mech.* **240**, 1–30.

Jiménez, J., Moffatt, H. K. & Vasco, C. 1996 The structure of the vortices in freely decaying two dimensional turbulence. *J. Fluid Mech.* **313**, 209–222.

Jiménez, J., Wray, A. A., Saffman, P. G. & Rogallo, R. S. 1993 The structure of intense vorticity in homogeneous isotropic turbulence. *J. Fluid Mech.* **255**, 65–90.

Kawahara, G., Kida, S., Tanaka, M. & Yanase, S. 1998 Wrap, tilt and stretch of vorticity lines around a strong thin straight vortex tube in a simple shear flow. *J. Fluid Mech.* **353**, 115–162.

Landman, M. J. & Saffman, P. G. 1987 The three-dimensional instability of strained vortices in a viscous fluid. *Phys. Fluids* **30**, 2339–2342.

Leblanc, S. & Cambon, C. 1998 Effects of the Coriolis force on the stability of Stuart vortices. *J. Fluid Mech.* **356**, 353–379.

Le Dizès, S., Rossi, M. & Moffatt, H. K. 1996 On the three-dimensional instability of elliptical vortex subjected to stretching. *Phys. Fluids* **8**, 2084–2090.

Leibovich, S. & Holmes, P. 1981 Global stability of the Burgers' vortex. *Phys. Fluids* **24**, 548–549.

Leweke, T. & Williamson, C. H. K. 1998*a* Cooperative elliptic instability of a vortex pair. *J. Fluid Mech.* **360**, 85–119.

Leweke, T. & Williamson, C. H. K. 1998*b* Three-dimensional instabilities in wake transition. *Eur. J. Mech.* B/*Fluids* **17**, 571–586.

Lifschitz, A. & Fabijonas, B. 1996 A new class of instabilities of rotating fluids. *Phys. Fluids* **8**, 2239–2241.

Lifschitz, A. & Hameiri, E. 1991 Local stability conditions in fluid dynamics. *Phys. Fluids* A **3**, 2644–2651.

Lundgren, T. S. 1982 Strained spiral vortex model for turbulent fine structure. *Phys. Fluids* **25**, 2193–2203.

Malkus, W. V. R. 1989 An experimental study of global instabilities due to tidal (elliptical) distortion of a rotating elastic cylinder. *Geophys. Astrophys. Fluid Dyn.* **48**, 123–134.

Miyazaki, T. & Fukumoto, Y. 1992 Three-dimensional instability of strained vortices in stably stratified fluid. *Phys. Fluids* A **4**, 2515–2522.

Moffatt, H. K., Kida, S. & Ohkitani, K. 1994 Stretched vortices -the sinews of turbulence; large-Reynolds-number asymptotics. *J. Fluid Mech.* **259**, 241–264.

Moore, D. W. & Saffman, P. G. 1975 The instability of a straight vortex filament in a strain field. *Proc. R. Soc. Lond.* A **346**, 413–425.

Peckham, D. H. & Atkinson, S. A. 1957 Preliminary results of low speed wind tunnel tests on Gothic wing of aspect ratio 1.0. *Aero. Res. Counc.* CP 508 (16–17).

Pierrehumbert, R. T. 1986 Universal short-wave instability of two-dimensional eddies in an inviscid fluid. *Phys. Rev. Lett.* **57**, 2157–2160.

Prochazka, A. & Pullin, D. I. 1995 On the two-dimensional stability of the axisymmetric Burgers vortex. *Phys. Fluids* **7**, 1788–1790.

Prochazka, A. & Pullin, D. I. 1998 Structure and stability of non-symmetric Burgers vortices. *J. Fluid Mech.* **363**, 199–228.

Robinson, A. C. & Saffman, P. G. 1984 Stability and structure of stretched vortices. *Stud. Appl. Math.* **70**, 163–181.

Rossi, M. & Le Dizès, S. 1997 Three-dimensional stability spectrum of stretched vortices. *Phys. Rev. Lett.* **78**, 2567–2569.

Saffman, P. G. 1992 *Vortex Dynamics*. Cambridge University Press.

Sarpkaya, T. 1971 On stationary and travelling vortex breakdowns. *J. Fluid Mech.* **45**, 545–559.

Sipp, D. & Jacquin, L. 1998 Elliptic instability in 2-D flattened Taylor-Green vortices. *Phys. Fluids* **10**, 839–849.

Ting, L. & Tung, C. 1965 Motion and decay of a vortex in a nonuniform stream. *Phys. Fluids* **8**, 1039–1051.

Tsai, C.-Y. & Widnall, S. E. 1976 The stability of short waves on a straight vortex filament in a weak externally imposed strain field. *J. Fluid Mech.* **73**, 721–733.

Van Dyke, M. 1975 *Perturbation Method in Fluid Mechanics*. Stanford: The Parabolic Press.

Verzicco, R., Jiménez, J. & Orlandi, P. 1995 On steady columnar vortices under local compression. *J. Fluid Mech.* **299**, 367–388.

Vincent, A. & Meneguzzi, M. 1991 The spatial structure and statistical properties of homogeneous turbulence. *J. Fluid Mech.* **225**, 1–20.

Vladimirov, V. A. & Tarasov, V. F. 1982 Structure of flow of a viscous liquid with closed streamlines. *Sov. Phys. Dokl.* **27**, 17–19.

Waleffe, F. 1989 The 3D instability of a strained vortex and its relation to turbulence. PhD thesis, Massachusetts Institute of Technology.

Waleffe, F. 1990 On the three-dimensional instability of strained vortices. *Phys. Fluids* A **2**, 76–80.

Widnall, S. E., Bliss, D. & Tsai, C.-Y. 1974 The instability of short waves on a vortex ring. *J. Fluid Mech.* **66**, 35–47.

Williamson, C. H. K. 1996 Three-dimensional wake transition. *J. Fluid Mech.* **328**, 345–407.